Numerical Simulation of UV Charging of Fractal Aggregates

Megan D. Marshall, Theresa Ma, Lorin S. Matthews, and Truell W. Hyde, *Member, IEEE*

***Abstract*—Dusty plasmas are a very common environment in the universe. This study uses is a numerical simulation of a dusty plasma with ultraviolet irradiance to calculate the charge on dust grains. The radiation creates a current of electrons that escape the aggregate due to the photoelectric effect. The model was developed from a previous code used to model complex plasmas that used a Line of Sight approximation of Orbital Motion Limited theory. Small aggregates were charged to equilibrium while irradiated by a photon flux of 10^{10} to 10^{18} $cm^{-2} \cdot s^{-1}$. The data produced shows that larger aggregates collect more charge and where the charging scheme switches from being electron current dominated at low fluxes, to photoelectron current dominant at high fluxes. This model proved to be an effective simulation of the charging that takes place in a dusty plasma with photoelectric currents caused by ultraviolet radiation.**

I. Introduction

Much of the universe is comprised of plasma. This plasma contains many small particles and aggregates of particles, creating complex plasmas [1], [2]. Because of the ubiquity of this environment, the field of complex plasmas is very important to the study of our universe and has become very popular recently, particularly as more of our solar system is being explored [3].

These particles are particularly interesting in space plasmas because they can coalesce and form aggregates that can eventually form planetesmals, which collide to create planets [1]. Other environments where dusty plasmas are found includes comet tails, stellar nebulae, and planetary and lunar atmospheres [3]. Because of the ionized environment the particles are in, they become charged [4], which affects the formation of aggregates and the size that they can reach [2], prompting the study of the charging properties through both numerical and laboratory experiments. There are many things that affect the charge on a aggregate in a complex plasma. These include properties of the plasma such as composition and temperature, aggregate constituents, and phenomena that affect the electric currents in the plasmas, including secondary electron emission and ultraviolet (UV) irradiation of the plasma [1], [2], [3], [4].

This paper will focus on the effects of UV radiation on aggregate charging. Using numerical simulations, previously built fractal aggregates were charged in the presence of UV radiation varying from 10^{10} to 10^{18} $cm^{-2} \cdot s^{-1}$. Plasma parameters were consistent with those used in a laboratory setting, and will be discussed along with the theory and methods used in this project in section II. Section III details the data collected from the simulations, which are discussed in section IV. The conclusions are presented in section V.

II. Theory

A. Orbital Motion Limited and Line of Sight

In a dusty plasma, the mobile ions and electrons form currents to the dust particles. Since the electrons are less massive than the ions, they will move faster and the negative current dominates, leading to negatively charged particles. One way to describe these currents is Orbital Motion Limited (OML) Theory. OML theory describes the closest approach these particles can make to a particle in plasma based on the principles of conservation of energy and momentum for the dust grain and the charged particle.

$$\begin{aligned} 1/2mv^2 &= 1/2mv_p^2 - q_e V_d && (1) \\ mvh_p &= mr_d v_p, && (2) \end{aligned}$$

where v_p is the velocity of the plasma species, r_d is the grain's radius, V_d is the potential on the grain, and

$$h_p = r_d\sqrt{1 + (V_d/V_0)}, \tag{3}$$

describes the closest approach of an electron or ion, known as the impact parameter, with V_0 is the initial potential of the plasma species [6]. Using a Maxwellian velocity distribution [5], [6], these equations are used to define the current due to charged particles. The current density for a given species of charged particles is [5]

$$J_\alpha = n_{\alpha\infty} q_\alpha \int_{v_{min},\alpha}^{\infty} f v^3 cos\theta d^2\Omega dv, \tag{4}$$

where $n_{\alpha\infty}$ is the number density of the plasma species far from the grain, q_α is the charge of the particle species (ion or electron), f is the Maxwellian distribution function, v is the velocity, θ is the angle of incidence with the grain surface, and $d^2\Omega$ is the solid angle around the grain [5]. The equilibrium charge for a dust grain can then be calculated by setting the sum of the currents to zero [5]. A line of sight (LOS) approximation was also used, which adjusts the current density equations around a particle by not including contributions from charged particles that would intersect with another particle, as explained in [5]. These contributions are evaluated by calculating the solid angle around a grain that is not blocked by other monomers, reducing $d^2\Omega$ for each obstructed path. After $d^2\Omega$ is found for each monomer, eqn. 4 is integrated, and the charging currents are found.

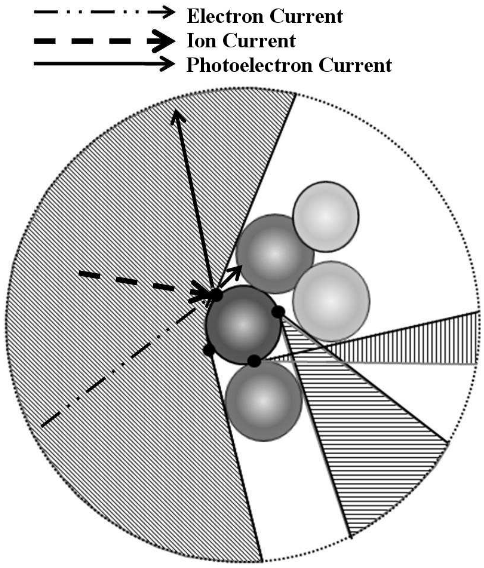

Fig. 1. Diagram of the LOS variation of OML theory with UV radiation included. The shaded regions indicate the area of velocity space where a charged particle can reach a dust grain without being blocked by another monomer, while the arrows represent the various currents. The arrows for the photoelectric currents demonstrate how the emitted electrons can be recaptured, depending on the grain's properties such as charge.

B. *UV charging*

When a plasma is irradiated by photons with energy in the UV range, electrons already present on the dust grains can be excited and, if the incident photon has enough energy to overcome the work function of the grain, escape due to the photoelectric effect. This creates a new current of photoelectrons in addition to the ion and electron currents of the plasma. The new current is a positive current, since the photoelectrons are leaving the grain. The emitted electrons can also be recaptured, if the grain is positively charged [1]. If the flux (ϕ) of photons is high enough to create a dominant photoelectric current, the grain can become positively charged [4]. To calculate the photoelectric current, the potential of the grain is found using

$$q_e V_d = k_B T \tag{5}$$

as in [1], k_B is Boltzmann's constant, and T is the temperature of the plasma. This gives a photoelectric current of [4]

$$I = \quad 4\pi r_p^2 \mu \phi \qquad V_d \leq 0 \tag{6}$$

$$I = \quad 4\pi r_p^2 \mu \phi e^{q_e V_d / k_B T} \qquad V_d > 0, \tag{7}$$

where μ is the photo emission efficiency (which is taken as 1 for metals and 0.1 for dielectrics). An illustration of the numerical modeling is shown in fig. 1.

In the numerical simulation, the electron, ion and photoelectron currents are calculated based on the potential of the aggregate. Using the LOS approximation, interactions between the aggregate and charged particles are calculated, and the new potential of the aggregate is found, and the currents are adjusted until the system reaches equilibrium. The addition of UV radiation means that previously collected electrons are released from the aggregate which have to be tracked not only to find the photoelectric current, but also to check for electron recapture if the emitted electrons collide with one of the monomers in the aggregate.

This code was used to charge 199 aggregates, ranging in size from two to 200 monodispersed particles that were previously built with only electron and ion charging. Each aggregate was charged with a range of photon fluxes from 10^{10} to 10^{18} $cm^{-2} \cdot s^{-1}$. Time steps were determined based on the size of the aggregate and the strength of the photon flux, ranging from 5x10^{-3} to 1x10^{-5} seconds, shown for each value of ϕ in Table I. These time steps were chosen based on previous charging experiments, then adjusted as needed to ensure that the aggregates were fully charged while preventing overcharging. Overcharging is when the charging history of an aggregate (examining the charge as a function of time) starts from a higher value than the equilibrium charge and asymptotically approaches the charge from a greater value rather than from zero. These time steps worked well for all sizes of aggregates, and were changed only when ϕ changed, though aggregate size does usually influence the time step length. The other parameters used are shown in Table II.

TABLE I
GOOD TIME STEPS

Photon Flux ($cm^{-2} \cdot s^{-1}$)	Time Step (s)
10^{10}	5x10^{-3}
10^{12}	5x10^{-3}
10^{13}	5x10^{-3}
10^{14}	1x10^{-3}
10^{15}	5x10^{-4}
10^{16}	5x10^{-4}
10^{17}	5x10^{-5}
10^{18}	1x10^{-5}

TABLE II
PARAMETERS THAT REMAINED CONSTANT THROUGH ALL AGGREGATE CHARGING

Parameter	Value
Plasma Constituents	H^+, e^-
Plasma Temperature (T)	4657 K
Plasma Number Density ($n_{\alpha\infty}$)	5x$10^8 m^{-3}$
Charge of Plasma Species (q_α)	$\pm$ e^-
Photoelectric Efficiency (μ)	0.1
Emitted Electron Temperature	11605 K
Dust Constituents	Silicate
Radius of a Single Grain (r_p)	6 μm

III. RESULTS

Once the equilibrium charge was reached by the aggregates, it was seen that the larger aggregates had more average charge than smaller ones, as seen in fig. 2. The charge for a given aggregate size was averaged over the 50 libraries that had been charged and was plotted versus N, the number of monomers in the aggregate. For ϕ =10^{10}, 10^{12}, 10^{13} and 10^{14} $cm^{-2} \cdot s^{-1}$, the absolute value of the average charge was taken for the plot, since these fluxes are in the electron current dominated region, making the actual charge on these aggregates negative. Notice that fig. 2 is plotted on a log-log scale. These averaged charge create a smooth increase in charge; however, the jump in the graph is due to the larger aggregates not reaching their equilibrium charge.

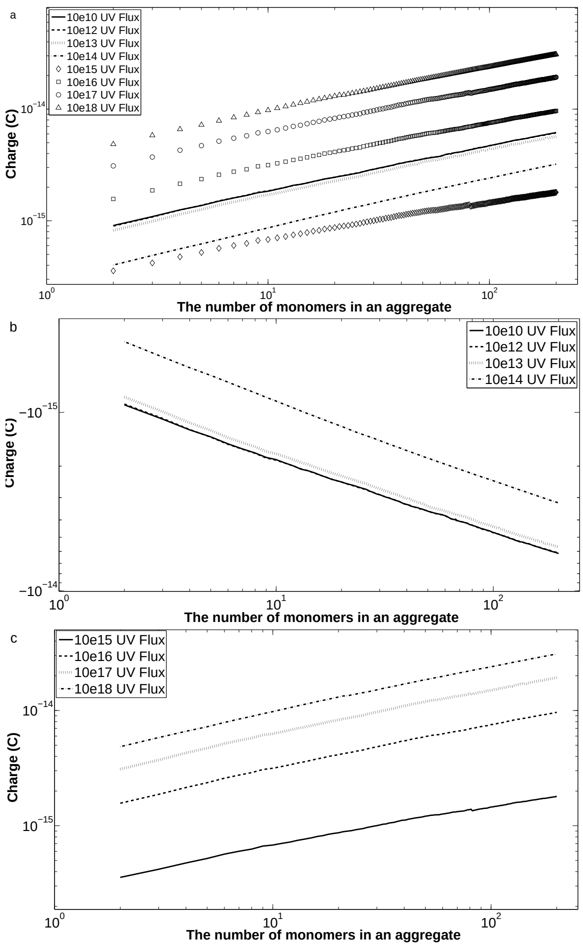

Fig. 2. Average charge versus number of monomers making up the aggregate. (a) shows the absolute value of the charges for ϕ = 10^{10} to 10^{14} $cm^{-2} \cdot s^{-1}$. (b) shows the plot of the negatively charged aggregates (ϕ = 10^{10} to 10^{14} $cm^{-2} \cdot s^{-1}$) while (c) shows the positively charge aggregates (ϕ = 10^{15} to 10^{18} $cm^{-2} \cdot s^{-1}$) The charge on each aggregate was averaged over all aggregates with the same N and was plotted against the number of monomers the aggregate has. For photon fluxes of 10^{10} $cm^{-2} \cdot s^{-1}$ to 10^{14} $cm^{-2} \cdot s^{-1}$, the absolute value of the average charge is plotted to make comparison across the various fluxes easier. As charging occurs, aggregates with more particles reach a higher charge. Due to shorter charging time, the larger aggregates did not reach the equilibrium charge, creating the drop in the curves at approximately 80 monomers. ϕ = 10^{14} $cm^{-2} \cdot s^{-1}$ and 10^{15} $cm^{-2} \cdot s^{-1}$ had the smallest absolute charge since these fluxes create photoelectric currents on the order of the negative electron current. ϕ = 10^{18} $cm^{-2} \cdot s^{-1}$ had the greatest absolute charge since it is far into the photoelectric dominant region.

Fig. 3 shows the charge versus the compactness of the aggregate. The compactness factor is used to describe how tightly arranged the monomers in an aggregate are. It is calculated using eq. 8 [7]

$$\phi_\sigma = N(r_p/R_\sigma)^3, \quad (8)$$

where N is the number of monomers in a given aggregate, r_0 is the radius of an individual monomer, and R_σ is the radius of the aggregate's average projected cross section, which is found using [7]

$$R_\sigma = \sqrt{\sigma/\pi}, \quad (9)$$

where σ is the area of the aggregate's projected cross section. Fluffier aggregates have a lower compactness factor. Note that the scale of the lower photon fluxes (Fig 3b) is an order of magnitude smaller than the higher ones (Fig 3a, 3c). Fig. 3 shows that there is a negative slope for charge versus compactness, meaning that the most compact aggregates have less charge than the larger ones. All sets of data have low scatter, with ϕ = 10^{10} $cm^{-2} \cdot s^{-1}$, 10^{12} $cm^{-2} \cdot s^{-1}$, and 10^{18} $cm^{-2} \cdot s^{-1}$ having the highest deviation from the trend line. ϕ = 10^{18} $cm^{-2} \cdot s^{-1}$ has the greatest slope, since this flux creates the highest average charge.

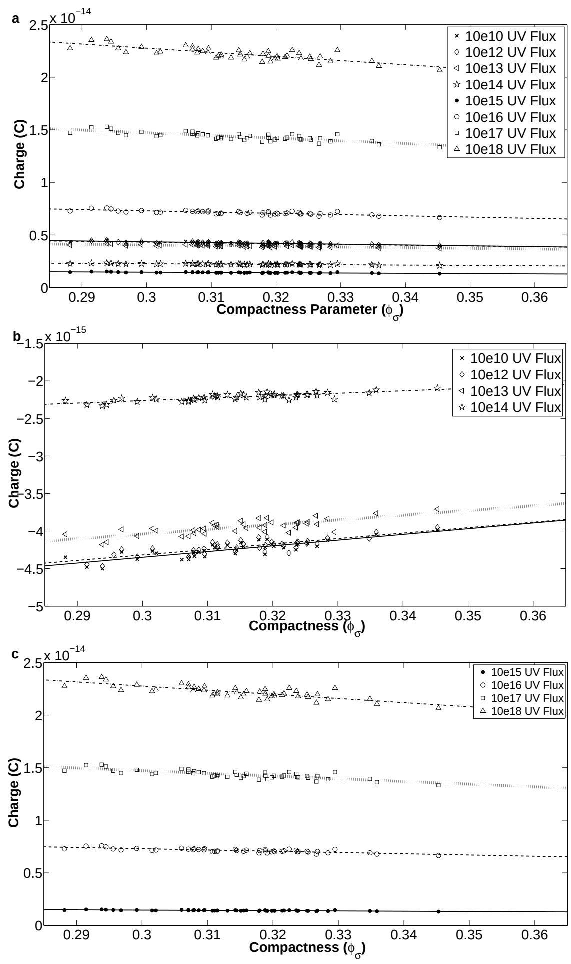

Fig. 3. Charge versus compactness factor for aggregates with N=200 monomers. Again (a) shows the absolute value of the charge, while (b) and (c) show the negative and positive charges, repespectively. The negative slopes shown in (a) indicates that larger aggregates (those with smaller compactness factors) have more charge than smaller ones. The smallest slopes were the fit lines for ϕ = 10^{14} and 10^{15} since they are in the region where the electron current and photoelectric current are comparable. ϕ = 10^{18} $cm^{-2} \cdot s^{-1}$ photon flux had the highest slope since it has the highest charge on average.

Fig. 4 show the potential of an aggregate plotted versus the radius. The potential was calculated by dividing the

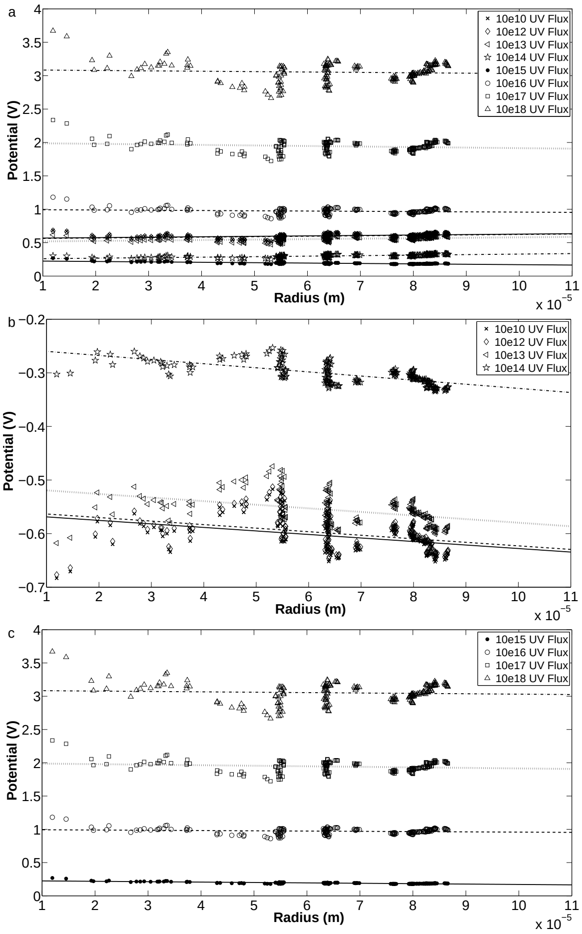

Fig. 4. Potential versus radius for a library of aggregates. Again (a) shows the absolute value of all the potentials, while (b) and (c) show the negative and positive values, respectively.One set of aggregates for each magnitude of flux had the potential of each aggregate calculated (by dividing charge by radius) and plotted against the radius of the aggregate. No significant trends were distinguishable between fluxes.

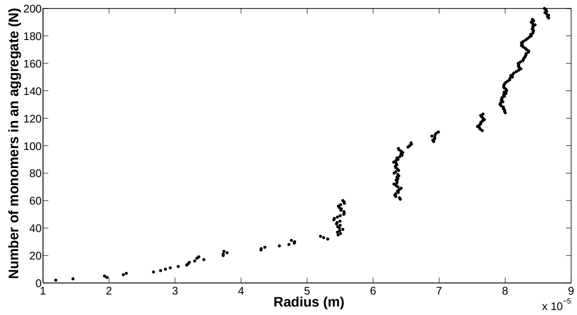

Fig. 5. N versus radius. The number of monomers in an aggregate is plotted versus the aggregate's radius to show the gaps in radius increase.

equilibrium charge by the radius for each aggregate. The radius for an aggregate is found by calculating the distance from the center of mass to each component monomer and setting the radius as the longest of these distances. For the plot, the same library of aggregates was chosen for consistency. There was a large spread in most of the plots, though ϕ = 10^{15} and 10^{16} $cm^{-2} \cdot s^{-1}$ have less scatter and are closer to their linear fits.

This particular set of aggregates has a gap in the radius around 0.6 μm. This is shown more clearly in fig. 5, which plots the aggregate radius versus N, the number of monomers in the aggregates. This also shows other smaller gaps in the radius. These developed during the aggregate formation, but it is not clear why, though it indicates that in areas, the aggregates become more compact as monomers are added before the radius increases.

IV. Discussion

In these simulations, it was seen that larger aggregates, both those with more monomers and those with smaller ϕ_σ, have greater charge (figs. 2, 3). This happens because the larger aggregates have more surface area which interacts more with the currents in the plasma. Additionally, the aggregates with a lower compactness factor have more space between the aggregates, creating even more area with which the currents can interact. This also means that higher UV fluxes can contact more of the aggregate, creating a larger photon flux.

The jumps in the plots of ϕ = 10^{15} and 10^{17} $cm^{-2} \cdot s^{-1}$ in fig. 3 is due to the larger aggregates not reaching their equilibrium charge. This happened because the simulation did not run long enough for sum of the currents around the aggregates to reach zero. For the other values of ϕ, this does not occur since the aggregates were fully charged before the simulation ended. This problem can easily be remedied by allowing the aggregates to charge for longer times, which can be accomplished by using a longer time step or extending the maximum time of the simulation. Time steps that worked best in this experiment are shown in table I.

The fluxes with the smallest charge, 10^{14} and 10^{15} $cm^{-2} \cdot s^{-1}$, are where the plasma changes from being dominated by the electron current, producing negatively charged aggregates, and dominated by the photoelectric current, creating positively charged aggregates. Fig. 4 also shows this shift from negative charging to positive, since the same values of photon flux have the lowest absolute potential. Since the photoelectric current is proportional to the photon flux, it seems that the switch between negative and positive charges occurs near ϕ=10^{15} $cm^{-2} \cdot s^{-1}$, since the charge and potential on grains are lower than that for ϕ=10^{14} $cm^{-2} \cdot s^{-1}$. This is more distinct for the larger aggregates, since the slope is higher for ϕ = 10^{14} $cm^{-2} \cdot s^{-1}$.

Fig. 4 has a large amount of scatter. It does indicate that the positively charged aggregates seem to have a slightly negative slope, indicating that they have a smaller potential at larger radii. This would suggest that the charge on the aggregates is smaller than the charge on an equivalent sphere.

V. Conclusion

The addition of UV charging to the OML simulations has allowed more situations and environments to be modeled. Not only can the code model laboratory experiments as described in this paper, but also locations in the solar system and throughout the universe where there is high UV radiation. The challenge using the code was ensuring the time step and maximum amount of time the aggregate charged were large enough for it to reach equilibrium without being so large that it overcharged.

The charge on an aggregate was seen to be proportional to the cross sectional area and the number of monomers composing the aggregate, since they have more interactions with both the currents in the plasma and the UV radiation. It also shows that fluxes between 10^{14} and 10^{15} $cm^{-2} \cdot s^{-1}$, the plasma changes from being dominated by the electron current to dominated by the photoelectric current, and that ϕ = 10^{15} $cm^{-2} \cdot s^{-1}$ or above creates positively charged aggregates.

In the future, it would be useful to develop a way to calculate a suitable time step for the charging and a way to determine when the equilibrium charge is reached to prevent the code from running longer than necessary. Also, the libraries should have the aggregates with more than 80 monomers recharged to eliminate the jump in the graphs. Further along the line, it would interesting to simulate cosmic environments such as the plasma around Saturn's rings or in the Earth's mesosphere to see if the code is able to accurately model them and provide insight into how they formed.

REFERENCES

[1] C.K. Goertz, "Dusty plasmas in the solar system," Reviews of Geophysics, vol. 27, no. 2, pp. 271-292, 1989.

[2] V.E. Fortov, A.G. Khrapak, S.A. Khrapak, V.I. Molotkov, and O.F. Petrov, "Dusty plasmas," Physics - Uspekhi, vol. 47, no. 5, pp. 447-492, 2004.

[3] D.A. Mendis, "Progress in the study of dusty plasmas," Plasma Sources Science and Technology, vol. 11, no. 3A, pp. 219-228, 2002.

[4] J. Goree, "Charging of particles in a plasma," Plasma Sources Science and Technology, vol. 3, no. 3, pp. 400-406, 1994.

[5] L.S. Matthews and T.W. Hyde, "Charging and growth of fractal dust grains," IEEE Transactions on Plasma Science, vol. 36, no. 1, pp. 310-314, 2008.

[6] J.E. Allen "Probe theory - the orbital motion approach," Physica Scripta, vol. 45, pp. 497-503, 1992.

[7] D. Paszun and C. Dominik, "Collisional evolution of dust aggregates. From compaction to catastrophic destruction," Astronomy and Astrophysics, vol. 507, no. 2, pp. 1023-1040, 2009.